Supporting Information

Facile Synthesis of MOF-Derived Ru-Doped Cobalt Oxide/Carbon Nanomaterials for Electrocatalytic Oxygen Evolution

Nan Li,[a,#] Rong Lin,[a,#] Yuchang Shen,[a] Haoran Wang,[a] Yuting Fu,[a] Qipeng Li,[b,*] and Jinjie Qian[a,*]

[a]Key Laboratory of Carbon Materials of Zhejiang Province, College of Chemistry and Materials Engineering, Wenzhou University, Wenzhou 325035, Zhejiang, P. R. China

[b]College of Chemistry and Chemical Engineering, Zhaotong University, Zhaotong 657000, Yunnan, P. R. China

[#]These authors contributed equally to this work.

*Corresponding author

E-mail: qpli@ztu.edu.cn (Q. Li); jinjieqian@wzu.edu.cn (J. Qian)

1. Experimental Details

1.1 Reagents and Materials.

Unless otherwise specified, chemicals are reagent grade and used directly without processing. Cobalt(II) acetate tetrahydrate ($Co(CH_3COO)_2 \cdot 4H_2O$, 99.5%, Aladdin), biphenyl-3,3',5,5'-tetra carboxylic acid (H_4BPTC, 98.0%, Jinan Henghua Technology Company), polyvinylpyrrolidone (PVP, ~58000, Aladdin), Ruthenium(III) chloride anhydrous ($RuCl_3$, Aladdin), N-Methylformamide (NMF, 99%, Aladdin), de-ionized water (18 MΩ), concentrated nitric acid solution (HNO_3, 70%, Aladdin), and ethanol (EtOH, 95%, Aladdin).

1.2 Synthesis of CoOF-1 ($[Co_2(OH)_2(BPTC)]$)

The mixture of $Co(CH_3COO)_2 \cdot 4H_2O$ (30 mg, 0.12 mmol), H_4BPTC (0.05 mmol, 15 mg), NMF (2 mL), and EtOH (1 mL) was added to a 35 mL pressure-resistant tube. Meanwhile, HNO_3 solution (0.3 mL) can adjust the mixture to be acidic condition. The reaction is then in an aluminum block bath to 140 ^oC for 4 hours. After cooling to room temperature, the product was centrifuged and collected, washed three

times with EtOH solution, and then the filtered solid was dried under vacuum at 85 ℃ overnight to obtain pure CoOF-1 in high yield.

1.3 Synthesis of CoOF-1-Co/C

The obtained CoOF-1 is weighed and placed in the a CVD tube furnace for the following thermal treatment. The temperature is set to 850 ℃ at a heating rate of 10 ℃ min^{-1} under an N_2 (50 sccm) atmosphere, and it is maintained at a constant temperature for another 2 hours. The black powders are obtained after falling to room temperature, denoted as CoOF-1-Co/C.

1.4 Synthesis of CoOF-1-RuCo/C

A mixture of Co/C (30 mg) and ethanol (3 mL) was added to a 35 mL pressure-resistant tube. Subsequently, 300 μL of $RuCl_3$ solution (Ru wt.% = 5 mg mL^{-1}) was transferred into the aforementioned mixture. The reaction was then carried out at 140 ℃ in an aluminum block bath for 4 hours. After naturally cooling to room temperature, the product was collected by centrifugation, washed three times with ethanol, and filtered. The resulting solid was dried overnight under vacuum at 85 ℃ to obtain CoOF-1-RuCo/C.

1.5 Synthesis of CoOF-1-RuCoO/C

The prepared CoOF-1-RuCo/C was weighed and placed in a muffle furnace. Subsequently, it was oxidized at different temperatures (200℃, 250℃, 300℃, and 350℃, respectively) in an air atmosphere, with a heating rate of 5℃ min^{-1}, and maintained for 2 hours. After cooling to room temperature, a black powder was obtained. The final products were named CoOF-1-RuCo/C-x (x = 200, 250, 300, 350) based on the oxidation temperature. The sample primarily characterized in this study is CoOF-1-RuCo/C-250, referred to as CoOF-1-RuCo/C for simplicity.

2. Material Characterization

The microscopic and nanostructured morphologies of all samples are characterized by scanning electron microscopy (SEM, JEOL JSM-6700F, 10 kV). The powder X-ray diffraction (PXRD) patterns are collected on a Bruker D8 Advance at 40 kV and 40 mA with Cu Kα radiation (λ=0.154 nm). Thermogravimetric analysis (TGA) is implemented under a flowing N_2 atmosphere by using a NETZSCH STA 449C unit. Raman spectrometer is investigated on LabRAM HR Evolution from the 532 nm line of an Ar-ion laser. X-ray photoelectron spectroscopy (XPS) is

recorded on a Thermo Scientific ESCALAB 250. Fourier transform infrared spectroscopy (FT-IR) spectra are carried on in the model of PerkinElmer Frontier MIR. N_2 adsorption/desorption isotherms are used to characterize the determine specific surface areas and pore distribution of samples based on the Brunauer-Emmett-Teller method (BET, Micrometrics ASAP 2020 system).

3. Electrochemical measurements

All electrochemical data were collected via the CHI760E and/or Autolab electrochemical workstation. OER measurements were performed in 1.0 M KOH solution using a typical three-electrode system, the GCE (glassy carbon electrode) with catalyst ink (geometric area: 1.5 cm^2), platinum mesh (geometric area: 0.0706 cm^2), and Hg/Hg_2Cl_2 electrode as the working electrode, counter electrode, and reference electrode, respectively. At the same time, we chose Hg/Hg_2Cl_2 as the reference electrode to ensure accuracy and reproducibility in alkaline media. All electrochemical tests in our work were performed without iR correction.

Briefly, the homogeneous catalyst ink was prepared by dispersing

2.5mg of catalyst powder into a mixed solution containing 75 μL of DI H_2O, 150 μL of ethanol and 25 μL of Nafion (5 wt.%), and then underwent an ultrasonic treatment for 1 h. 6 μL of the resultant catalyst ink was drop-casted onto the GCE electrode surface with a loading value of 0.85 mg cm^{-2},, and dried at room temperature. As a comparison, commercial RuO_2 also was tested.The linear sweep voltammetry (LSV) is collected with a scan rate of 5 mV s^{-1} after initial 40 circles cyclic voltammogram (CV) progress at a scan rate of 100 mV s^{-1} to have a stable CV curve.The electrochemical double-layer capacitance (C_{dl}) is measured by using CV in a non-Faradaic region (0.91-1.01 V vs. RHE) at different scan rates of 20, 40, 60, 80 and 120 mV s^{-1}. Electrocatalytic stability is made by using Amperometric curve (i-t) at a potential of 1.5 V vs. RHE for 48 h. In order to calculate the electron transfer number (N), rotating ring-disk electrode (RRDE) voltammogram of as-prepared samples are conducted to collect disk current (I_{disk}) and ring current (I_{ring}) at the same time, equation as follows: $N=4 \times I_d / (I_d + I_r / N_c)$, where I_r is the ring current, I_d is the disk current, and N_c is the current collection efficiency. The Faradaic efficiency (ε) is calculated by the equation as

follows: $\varepsilon = I_r /(I_d \cdot N_c)$.

4. Computational details

The density functional theory was used to carry out all the calculations with the Perdew-Burke-Ernzerh exchange-correlation functional of generalized gradient approximation and the projector-augmented wave method, which was implemented through Vienna Ab-initio Simulation Package (VASP).The input model structure file was created by VESTA.[1] The plane wave-basis expansion cutoff energy was fixed at 500 eV, and atomic relaxation was conducted until the force exerted on atoms was less than 0.05 eV $Å^{-1}$ and energy was concurrently converged to 1×10^{-5} eV. The k-point was a Monkhorst-Pack of 3×3×1.

The Gibbs free energy change (ΔG) of each lithiation step was defined as:

$$\Delta G = \Delta E + \Delta ZPE - T\Delta S,$$

where ΔE is the electronic energy difference directly obtained from DFT calculations, ΔZPE is the change in zero-point energy, T is the temperature (T= 298.15 K) and ΔS is the change in the entropy, respectively.[2] The zero-point energy and entropy were obtained through vibrational frequencies.

Conventionally, in an alkaline electrolyte, the anode reactions after oxygen adsorption can be written as:

$$H_2O \leftrightarrow OH^* + H^+ + e^- \quad (1)$$

$$OH^* \leftrightarrow O^* + H^+ + e^- \quad (2)$$

$$O^* + H_2O \leftrightarrow OOH^* + H^+ + e^- \quad (3)$$

$$OOH^* \leftrightarrow O_2^* + H^+ + e^- \quad (4)$$

[1]K. Momma, F. Izumi. VESTA 3 for three-dimensional visualization of crystal, volumetric and morphology data. J. Appl. Cryst., 2011, 44 , 1272-1276.

[2]J. Cao, X. Zhang, S. Zhao, X. Lu, H. Ma. Mechanism of the two-dimensional $WSeTe/Zr_2CO_2$ direct Z-scheme van der Waals heterojunction as a photocatalyst for water splitting. Phys. Chem. Chem. Phys., 2022, 24 , 21030-21039.

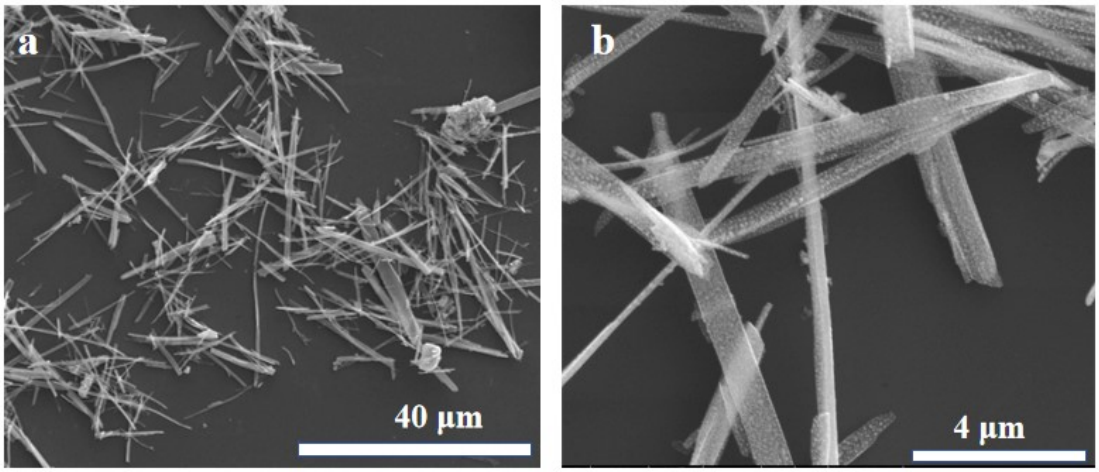

Fig. S1 SEM images of CoOF-1-Co/C.

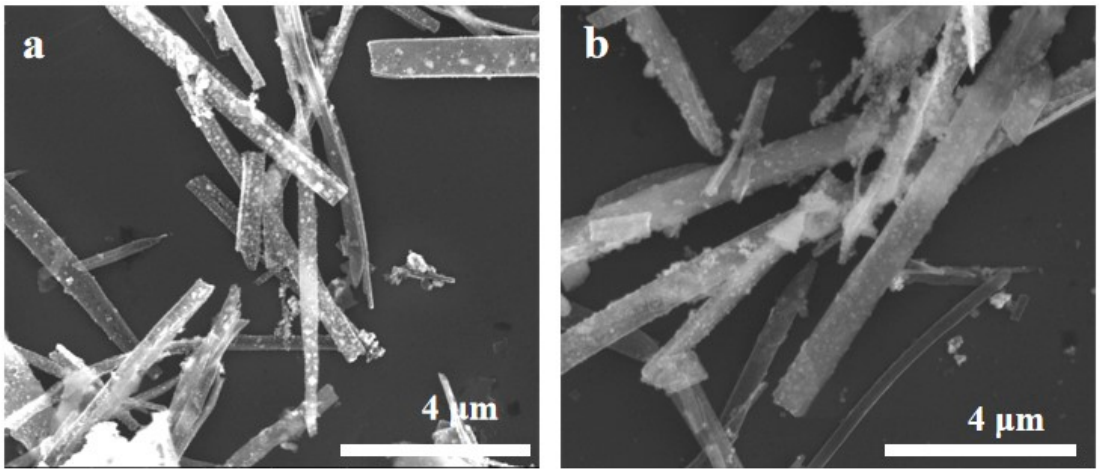

Fig. S2 SEM images of CoOF-1-RuCo/C.

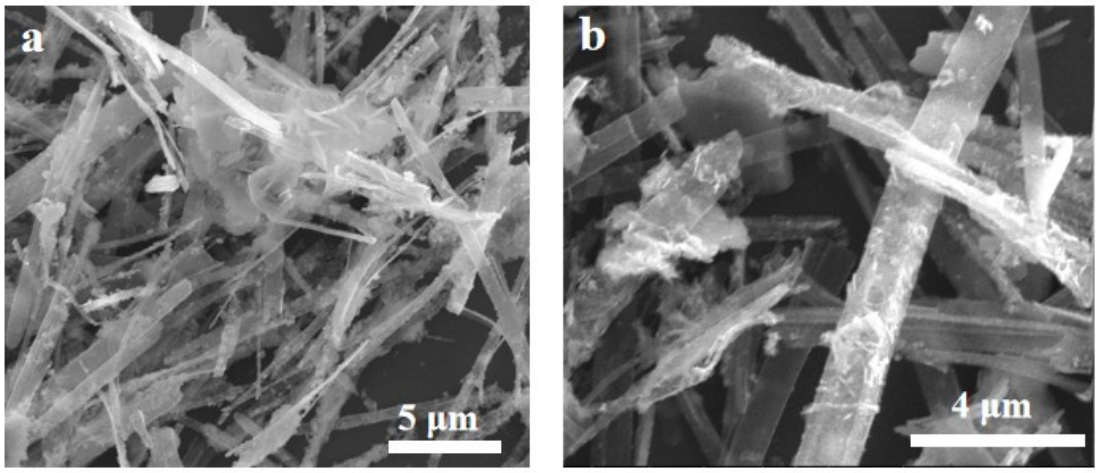

Fig. S3 SEM images of CoOF-1-RuCoO/C.

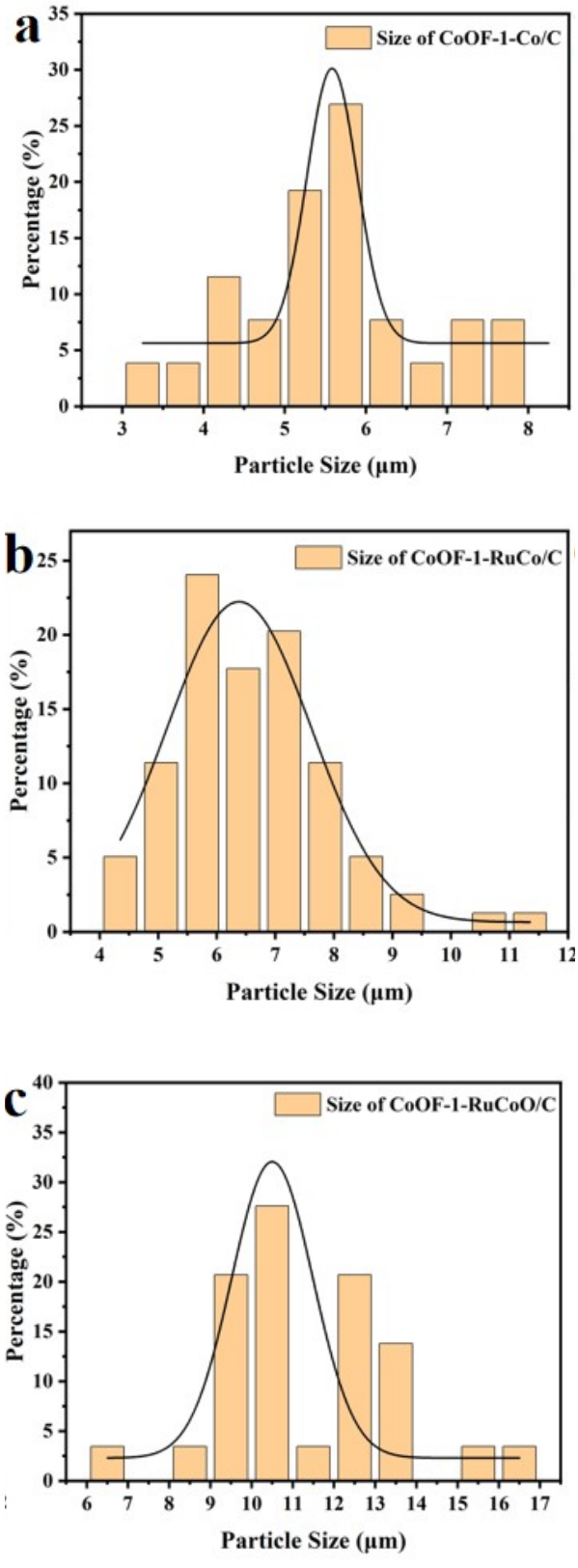

Fig. S4 Particle size distribution of (a) CoOF-1-Co/C, (b) CoOF-1-RuCo/C, (c) CoOF-1-RuCoO/C.

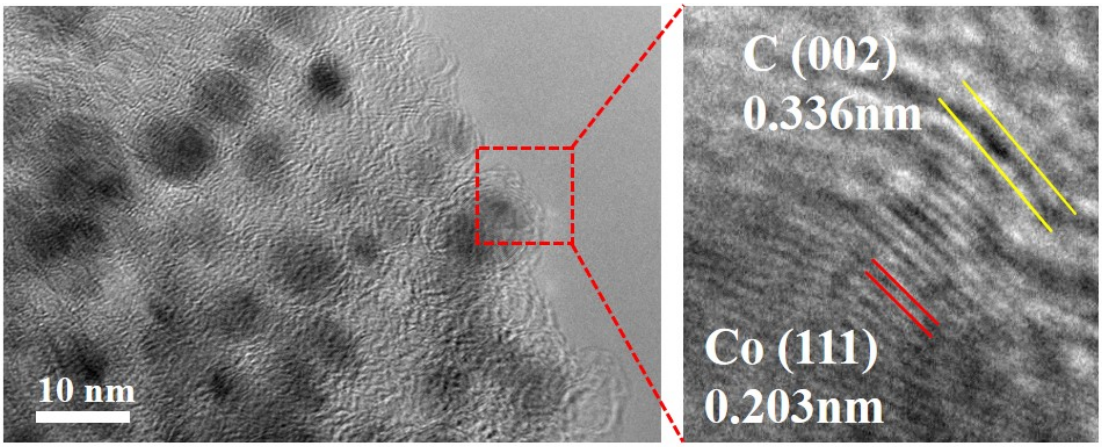

Fig. S5 TEM and HR-TEM images of CoOF-1-Co/C.

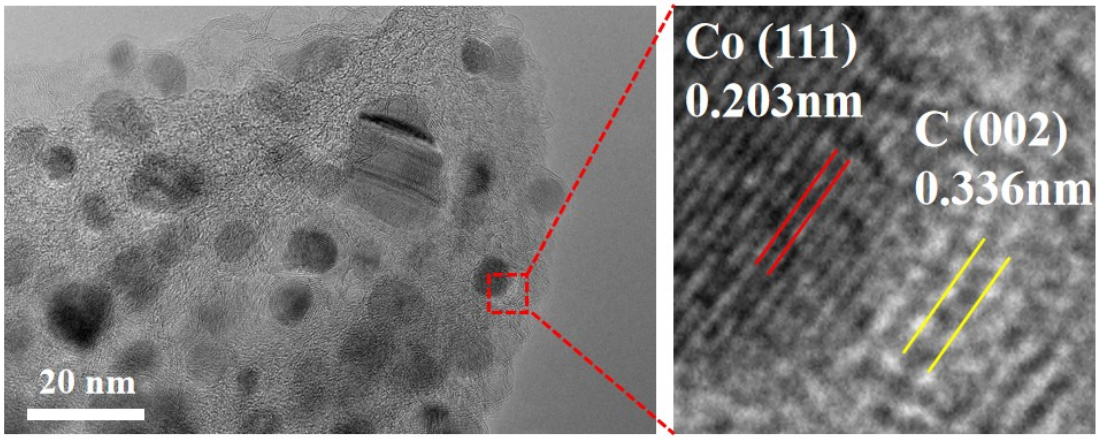

Fig. S6 TEM and HR-TEM images of CoOF-1-RuCo/C.

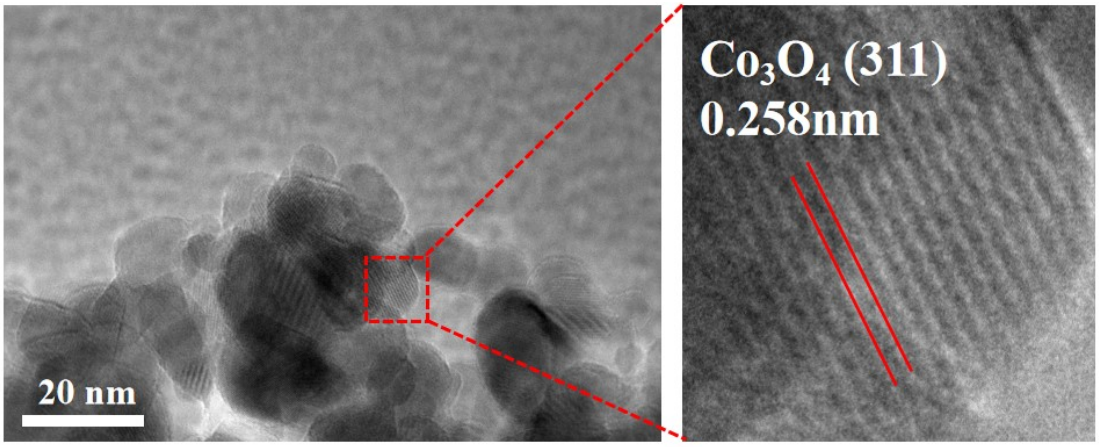

Fig. S7 TEM and HR-TEM images of CoOF-1-RuCoO/C.

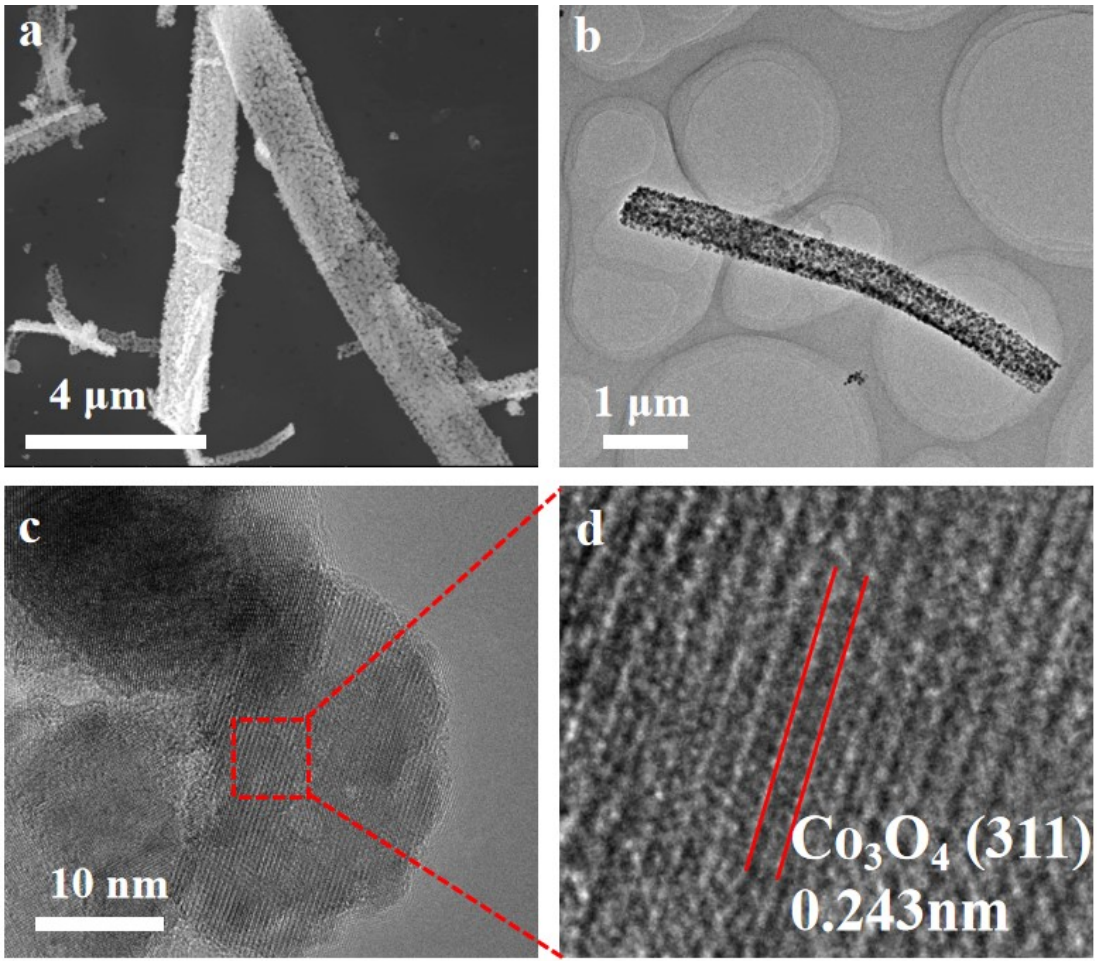

Fig. S8 SEM, TEM and HR-TEM images of CoOF-1-derived Co_3O_4 (CoOF-1-CoO).

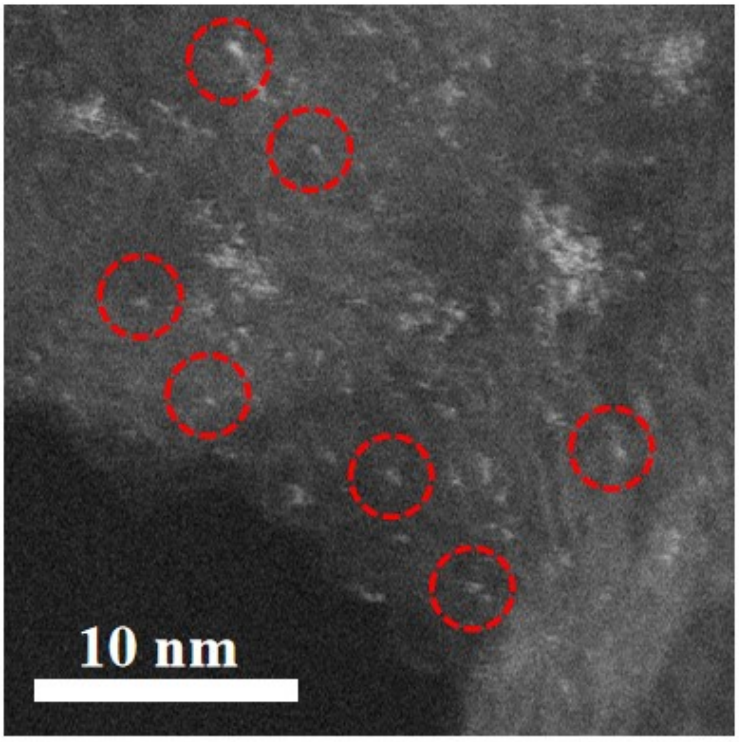

Fig. S9 AC-HAADF-STEM image of CoOF-1-RuCoO/C.

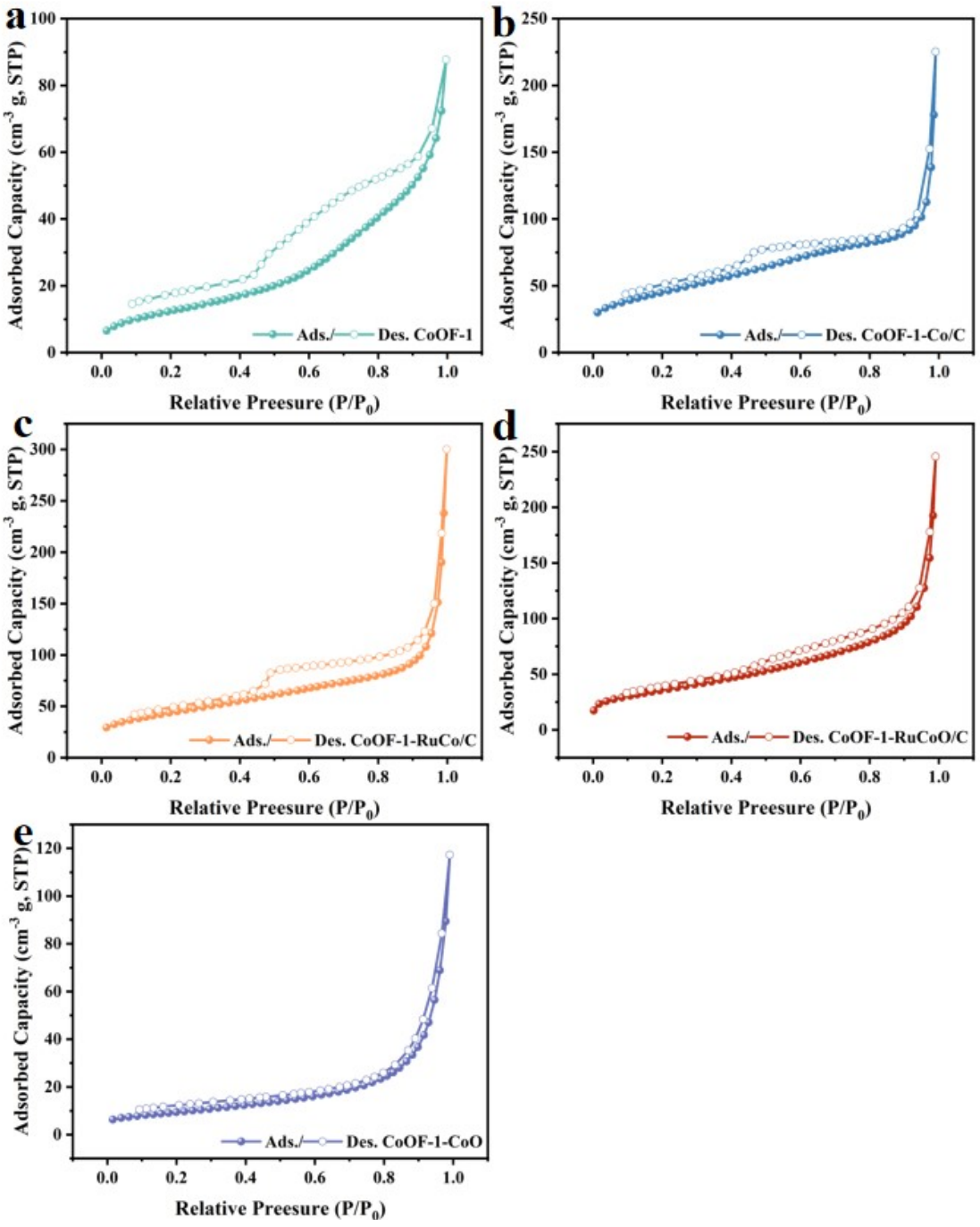

Fig. S10 N_2 adsorption/desorption isotherms of (a) CoOF-1, (b) CoOF-1-Co/C, (c) CoOF-1-RuCo/C, (d) CoOF-1-RuCoO/C, and (e) CoOF-1-CoO.

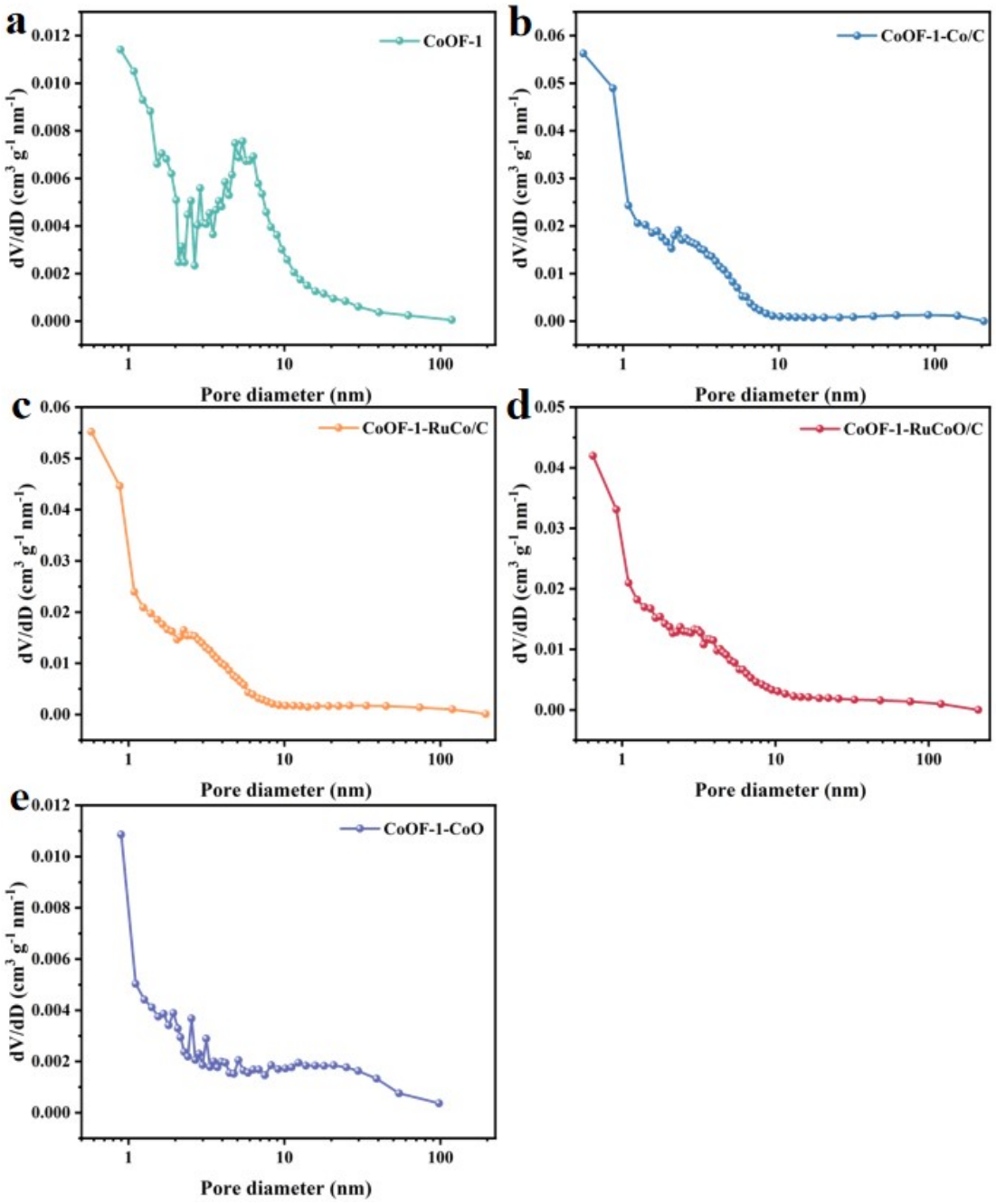

Fig. S11 PSD curves of (a) CoOF-1, (b) CoOF-1-Co/C, (c) CoOF-1-RuCo/C, (d) CoOF-1-RuCoO/C, and (e) CoOF-1-CoO.

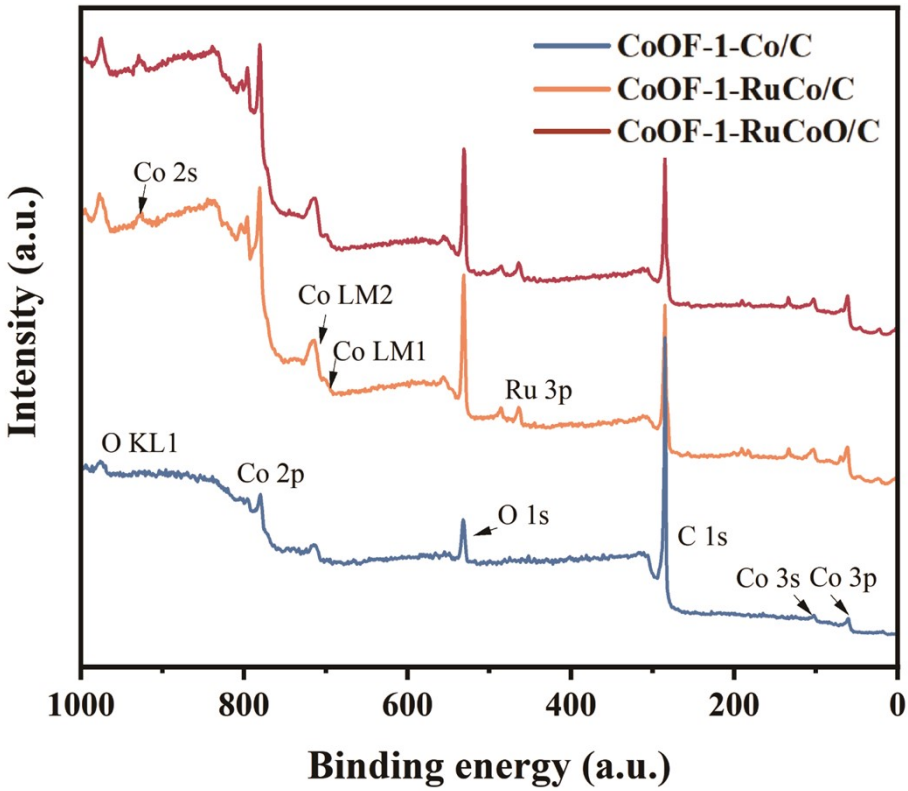

Fig. S12 XPS full spectra of CoOF-1-Co/C, CoOF-1-RuCo/C, and CoOF-1-RuCoO/C.

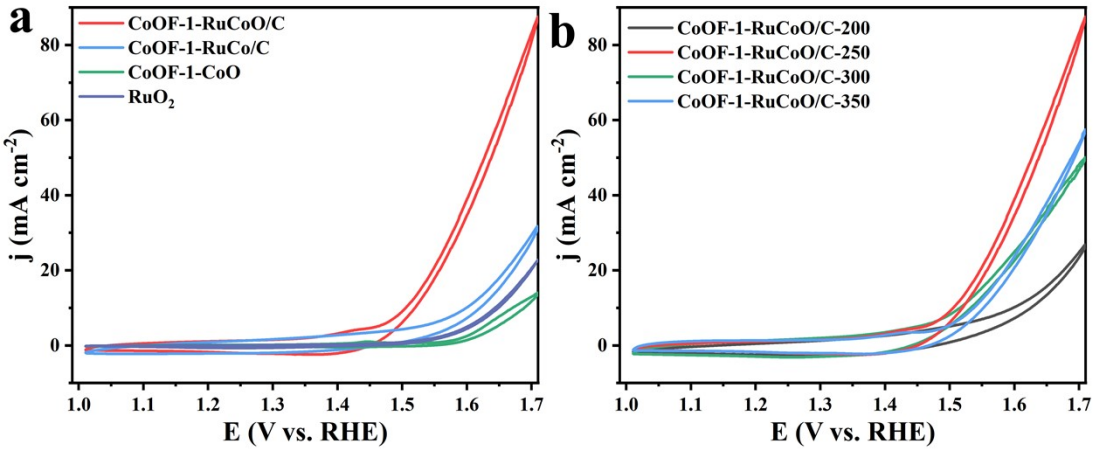

Fig. S13 Cyclic voltammetry curves of MOF-derived OER catalysts and commercial catalysts.

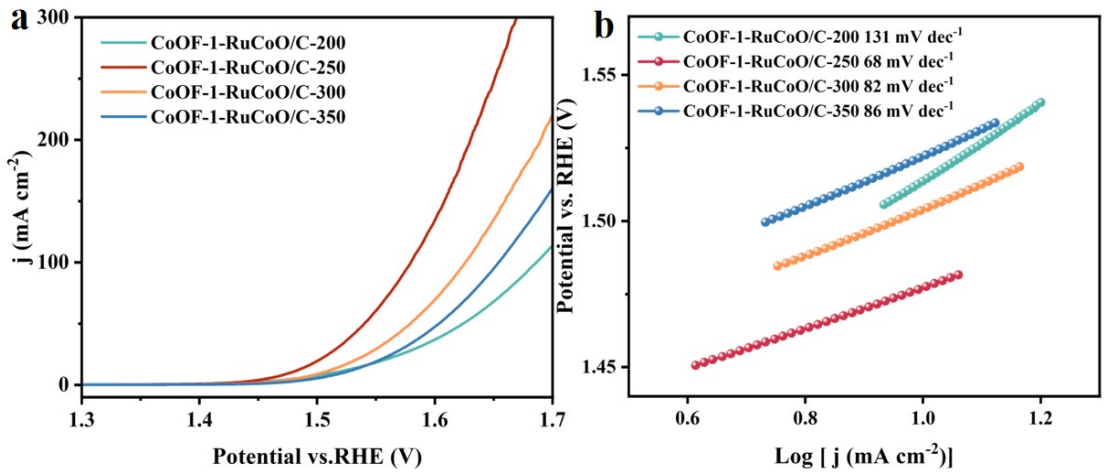

Fig. S14 Optimization of the OER performance: (a) LSV curves, and (b) Tafel slopes of CoOF-1-RuCoO/C with different oxidation temperatures.

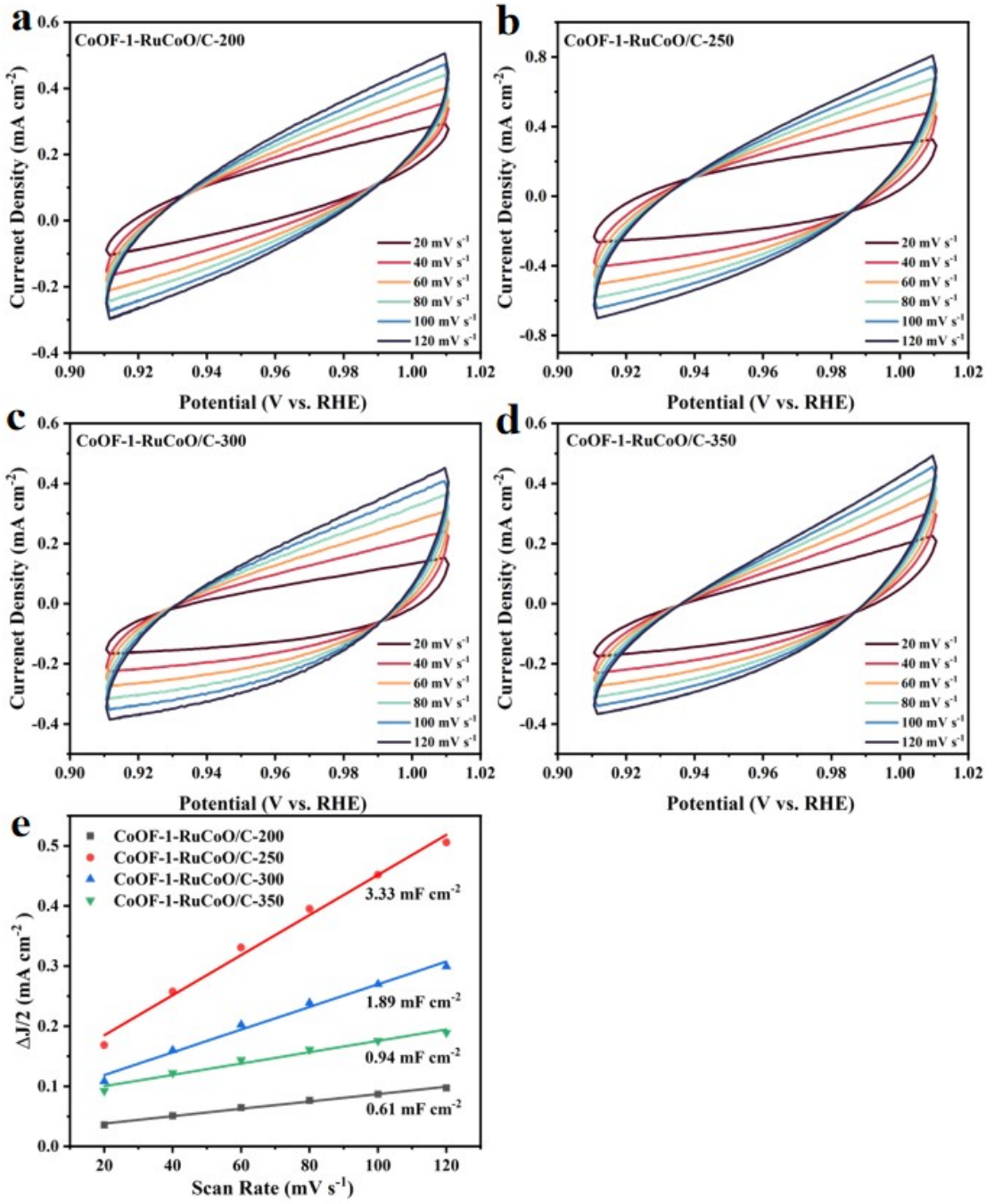

Fig. S15 Cyclic voltammograms of the CoOF-1-RuCoO/C at the temperatures of (a) 200 °C, (b) 250 °C, (c) 300 °C, (d) 350 °C, and (e) The calculated C_{dl} profiles.

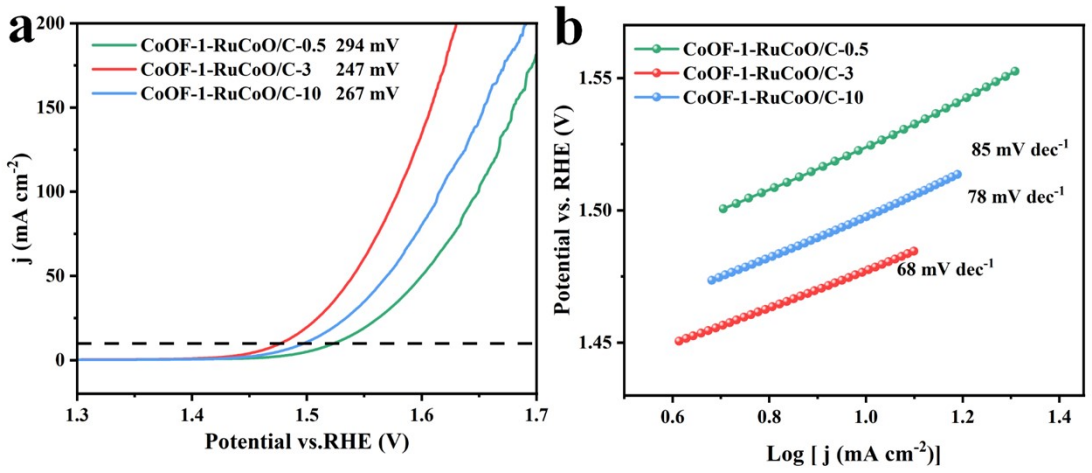

Fig. S16 Optimization of the OER performance: (a) LSV curves, and (b) Tafel slopes of CoOF-1-RuCoO/C series (x = 0.5, 3, 10) with different Ru contents (wt.%).

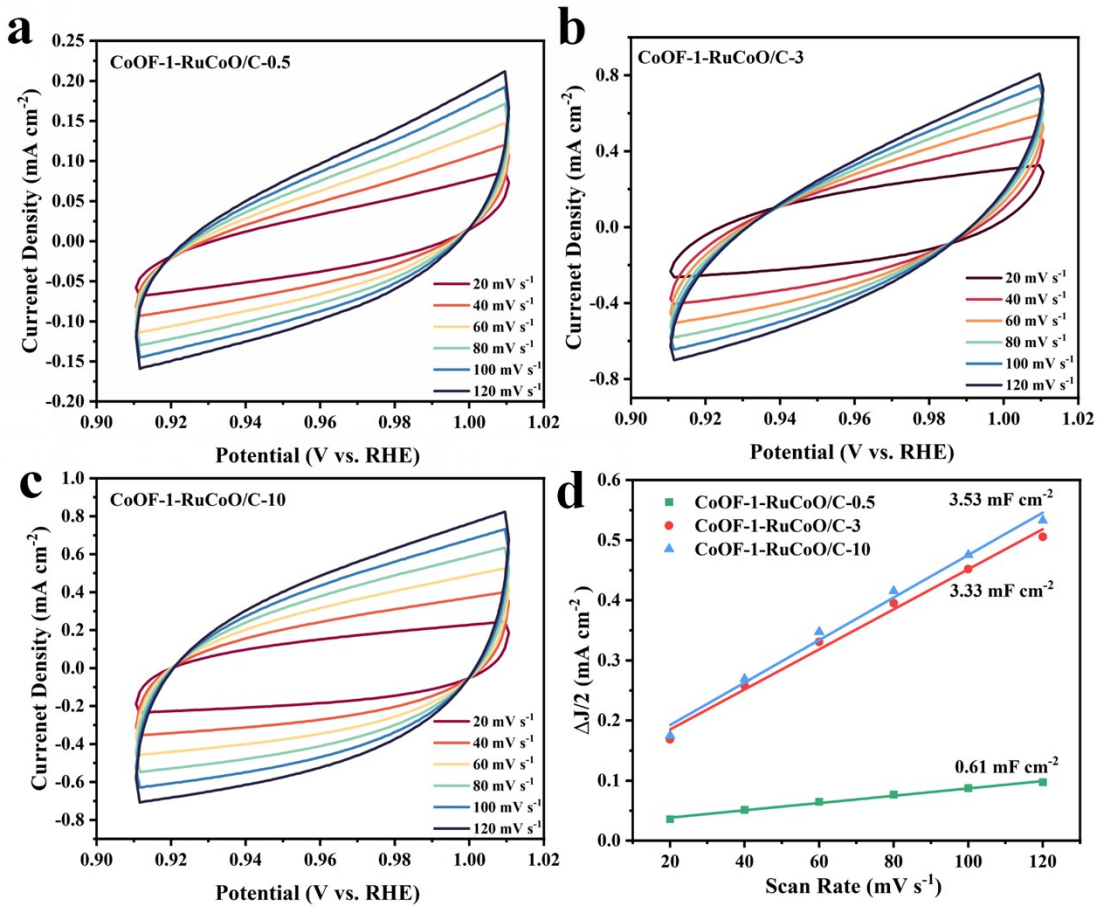

Fig. S17 CV curves of (a) CoOF-1-RuCoO/C-0.5, (b) CoOF-1-RuCoO/C-3, (c) CoOF-1-RuCoO/C-10 at different scanning rates, and (d) The calculated C_{dl} profiles.

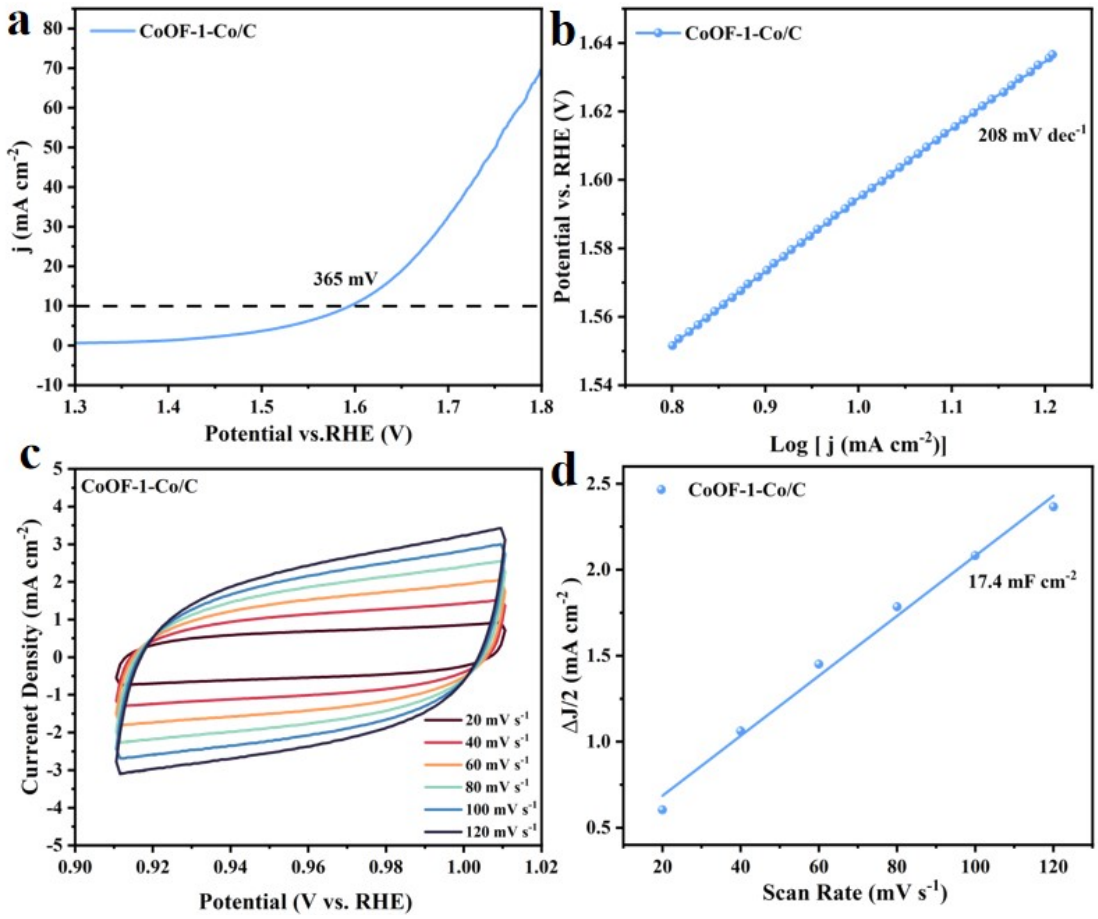

Fig. S18 (a) LSV curve, (b) Tafel slope, (c) CV curves at different sweep speeds from 20 to 120 mV s^{-1} and (d) C_{dl} profile of CoOF-1-Co/C.

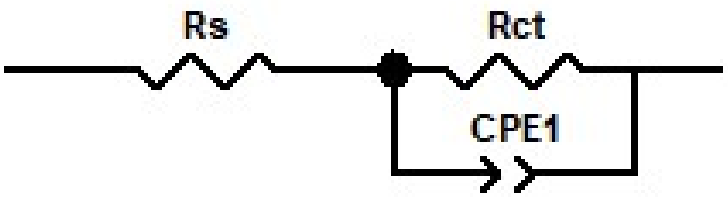

Fig. S19 The equivalent electrical circuit for EIS data (Rs: solution resistance; Rct and CPE1: resistance and CPE impedance of electrical double layer at the interface of activated product layer and GCE substrate).

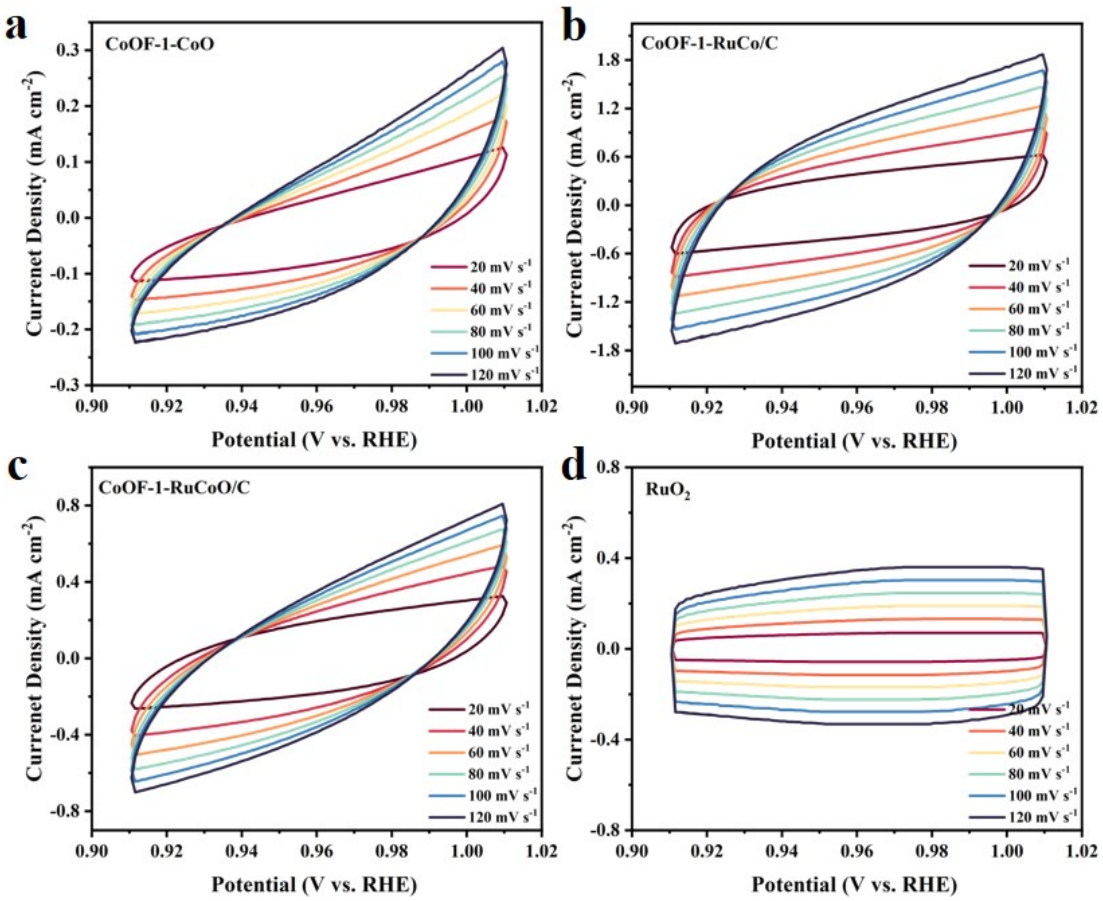

Fig. S20 The double-layer capacitance (C_{dl}) is calculated from the cyclic voltammograms of the (a) CoOF-1-Co/C, (b) CoOF-1-RuCo/C and (c) CoOF-1-RuCoO/C, (d) RuO_2.

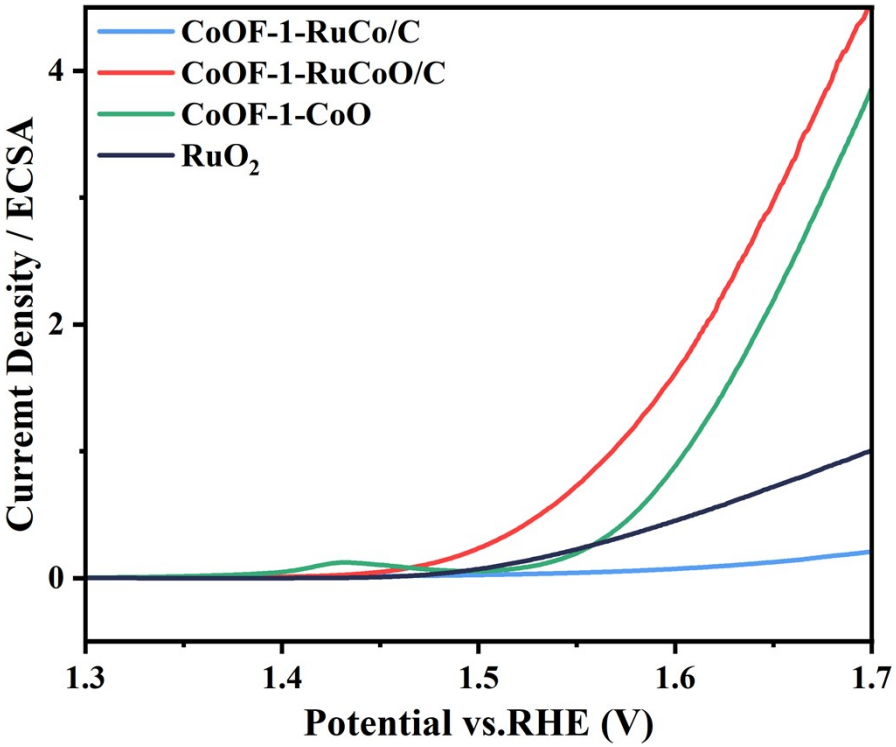

Fig. S21 The ESCA-normalized LSV curves of various electrocatalysts.

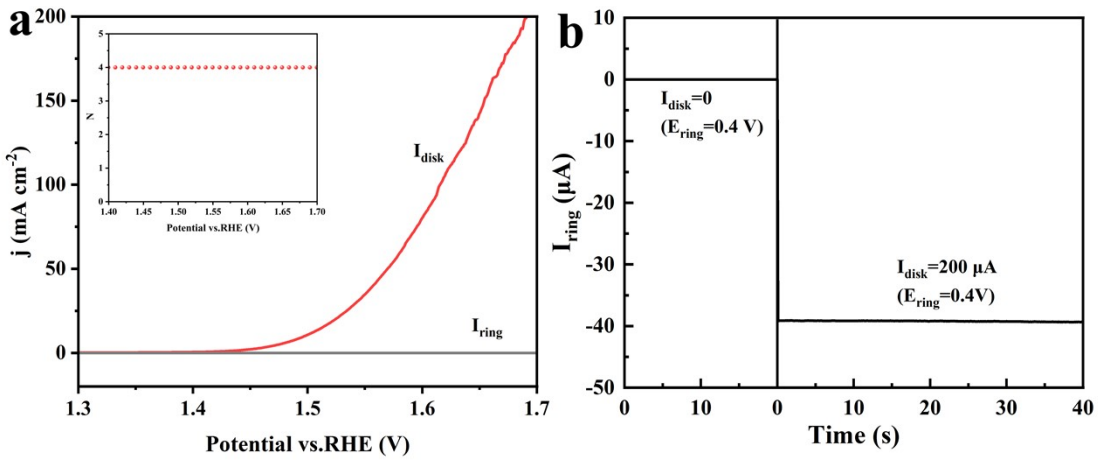

Fig. S22 (a) RRDE voltammogram and the calculated N for CoOF-1-RuCoO/C. (b) Ring current of CoOF-1-RuCoO/C.

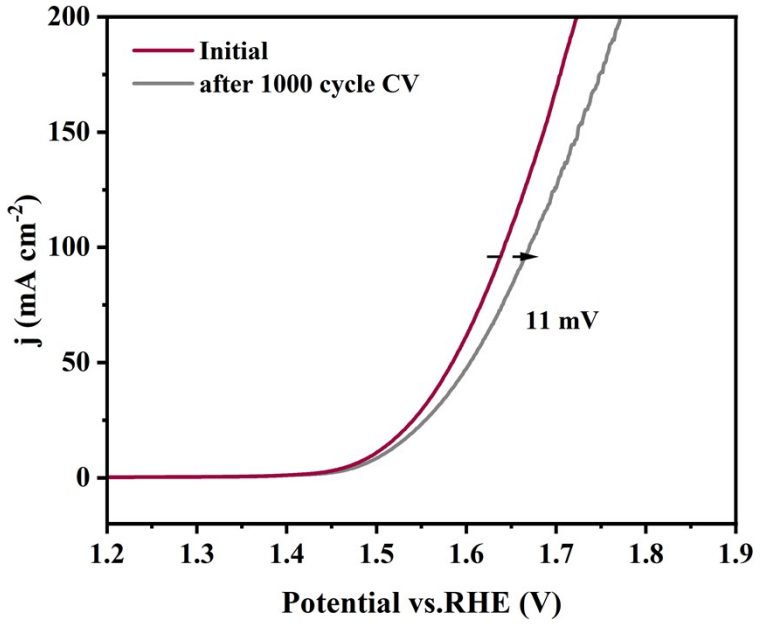

Fig. S23 LSV curves before and after 1000-cycle CV for CoOF-1-RuCoO/C.

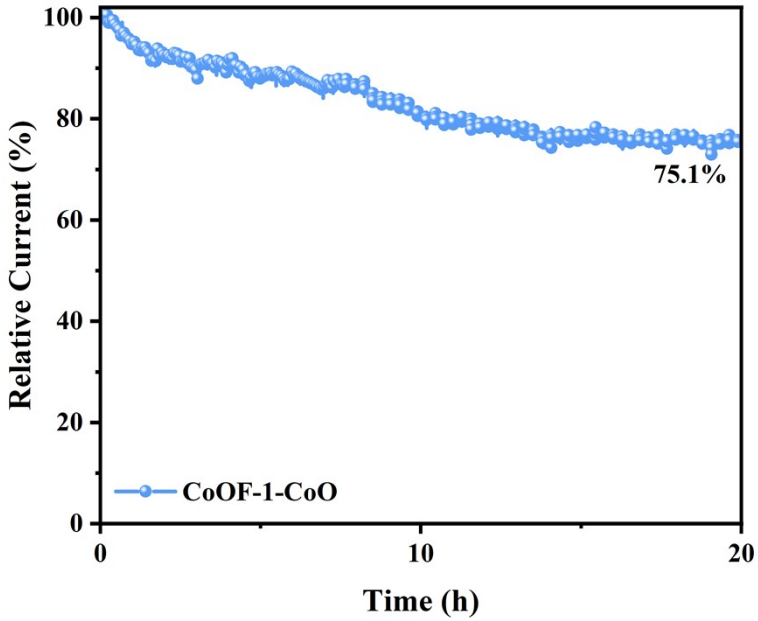

Fig. S24 The i-t stability test of CoOF-1-CoO.

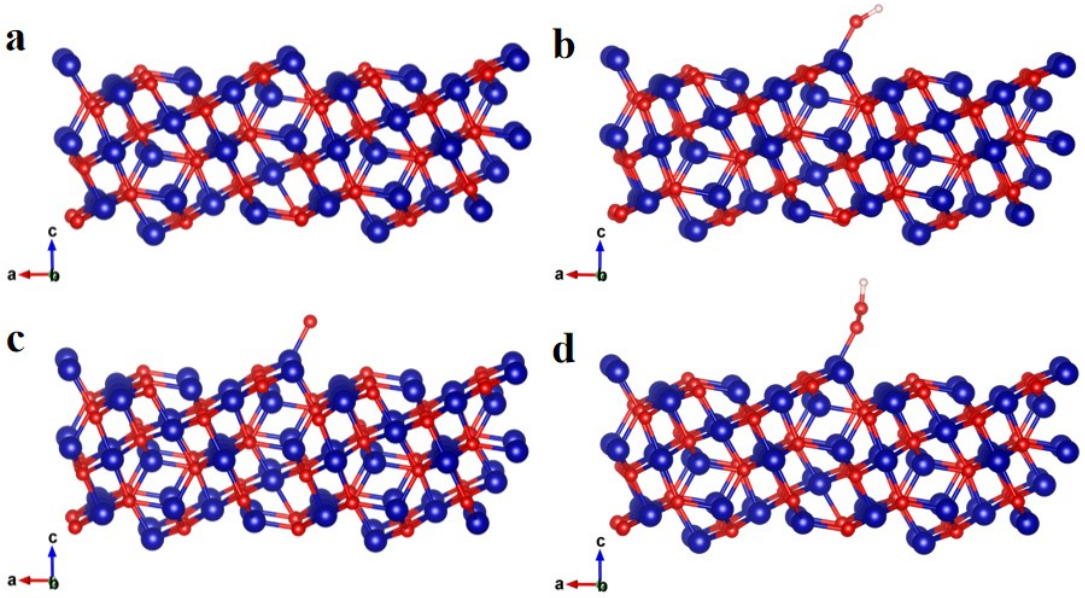

Fig. S25 The relaxation structure of each intermediate state of Co_3O_4 in AEM reaction pathways on Co site.

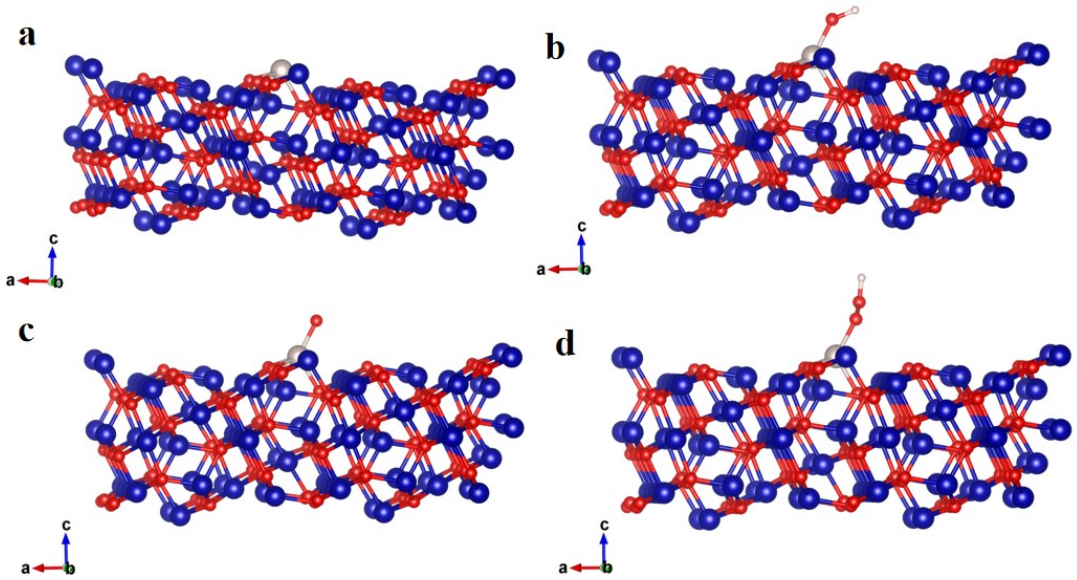

Fig. S26 The relaxation structure of each intermediate state of Ru-Co_3O_4 in AEM reaction pathways on Ru site.

For detailed OER procedure (**Figures S20-21**): In step I, the hydroxide ion was first adsorbed on the iron active site and loses one electron to form an adsorbed hydroxyl group. In step II, *OH was further oxidized and dehydrogenated to generate adsorbed oxygen atoms (*O) and release water molecules. Subsequently, through steps III-IV, the *OOH intermediate was formed and eventually desorbed to release oxygen, restoring the catalyst to its initial state.

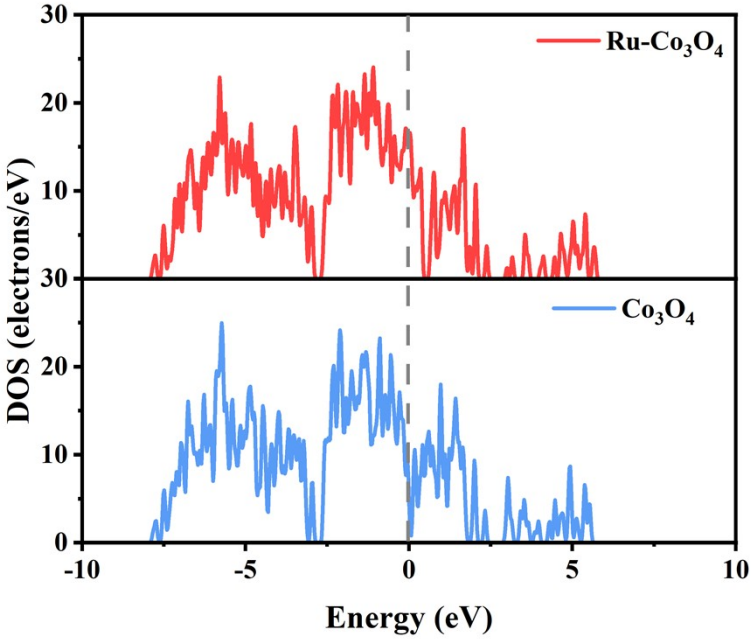

Fig. S27 DOS profiles of Co_3O_4 and Ru-Co_3O_4.

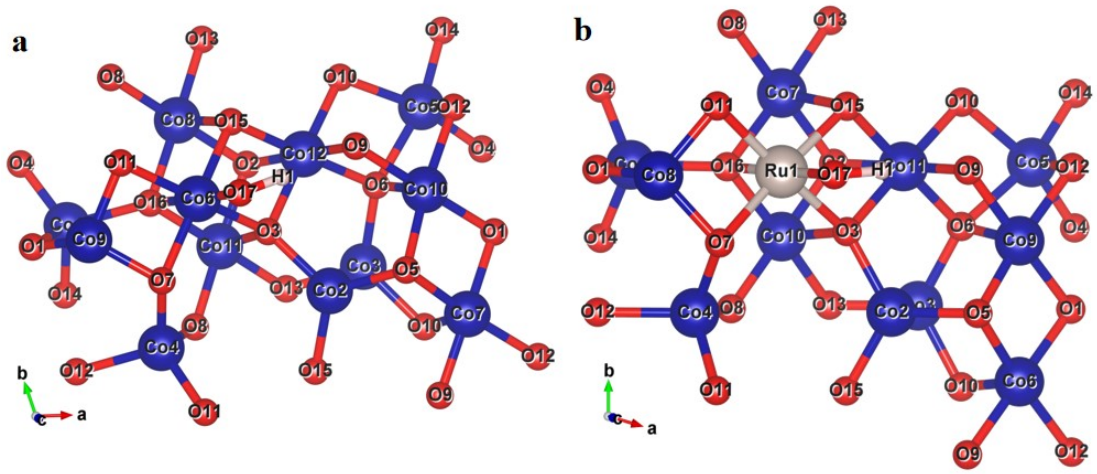

Fig. S28 Bader charge distribution diagrams of (a) Co_3O_4 and (b) Ru-Co_3O_4.

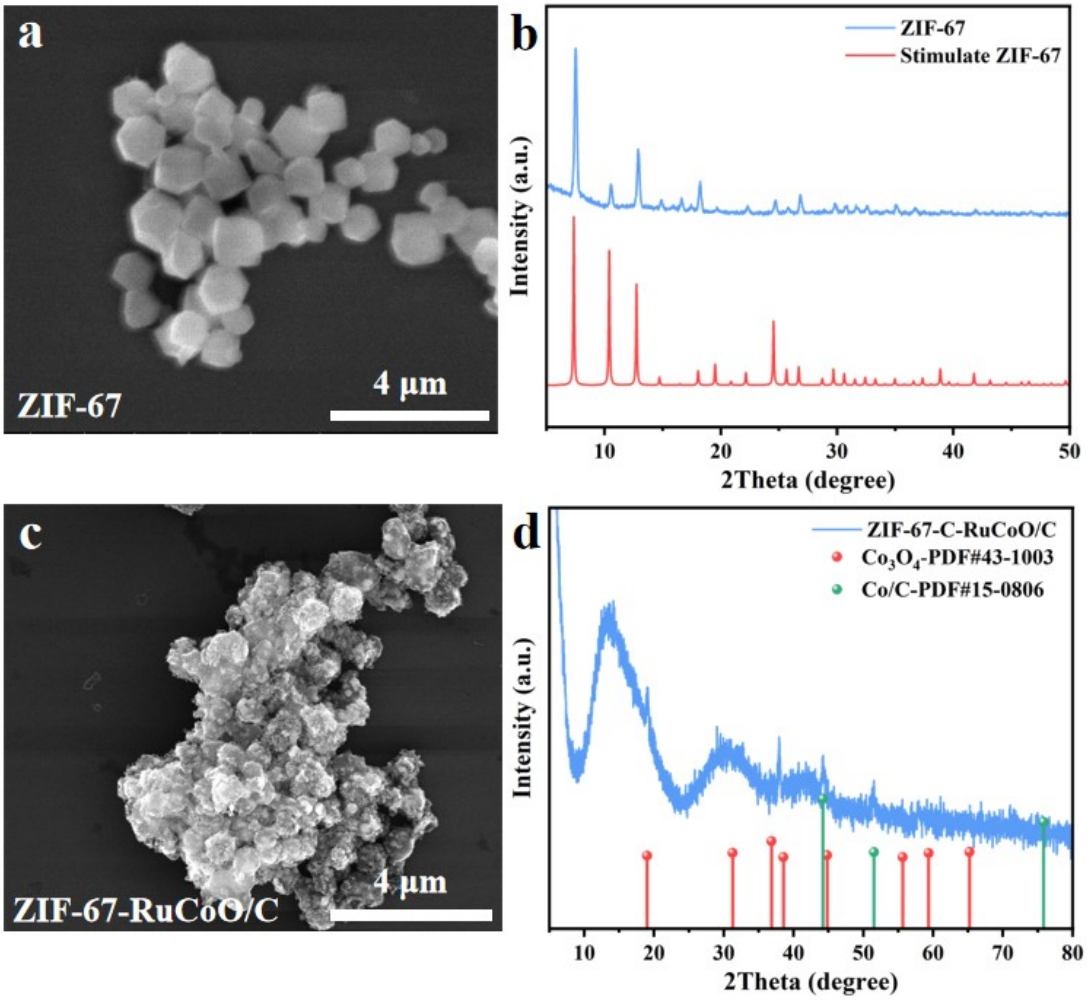

Fig. S29 (a) SEM image and (b) PXRD pattern of ZIF-67; (c) SEM image and (d) PXRD pattern of ZIF-67-RuCoO/C.

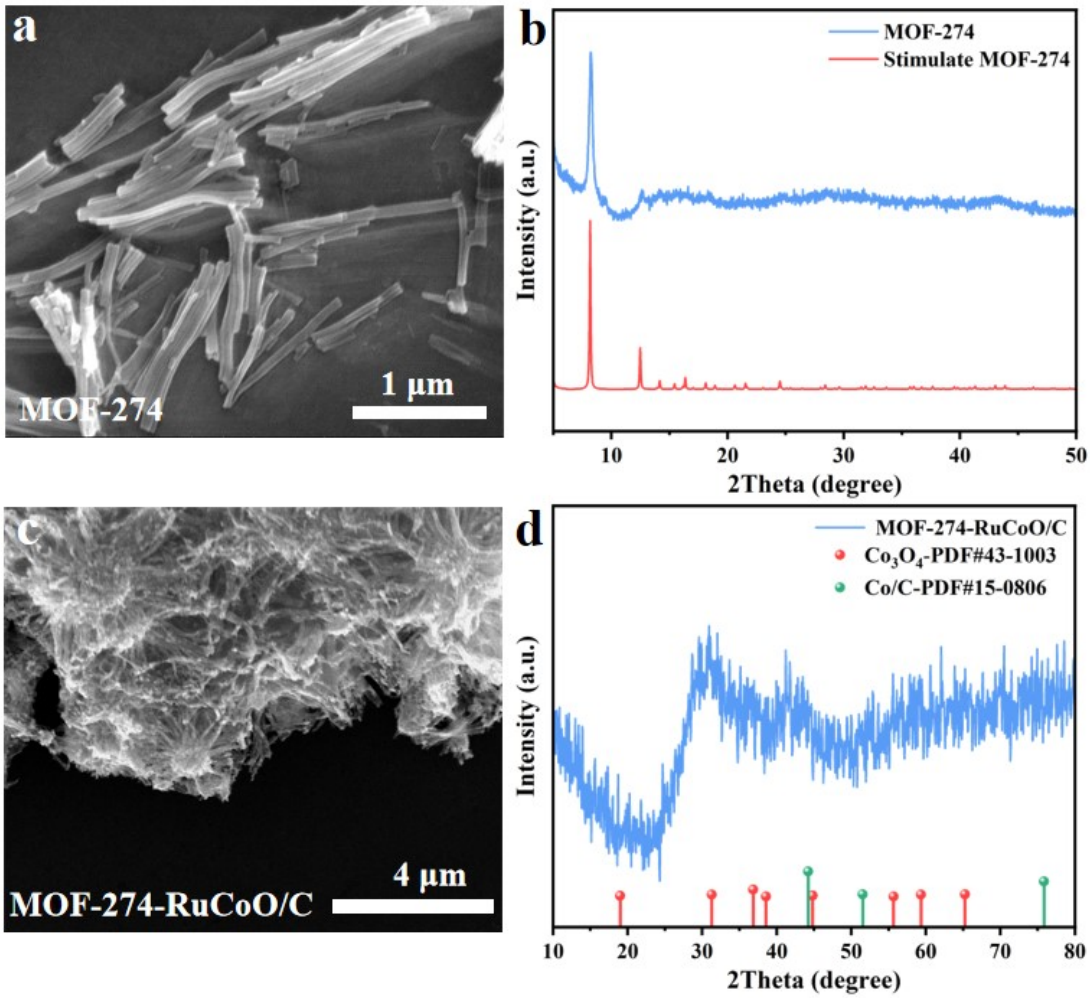

Fig. S30 (a) SEM image and (b) PXRD pattern of MOF-274; (c) SEM image and (d) PXRD pattern of MOF-274-RuCoO/C.

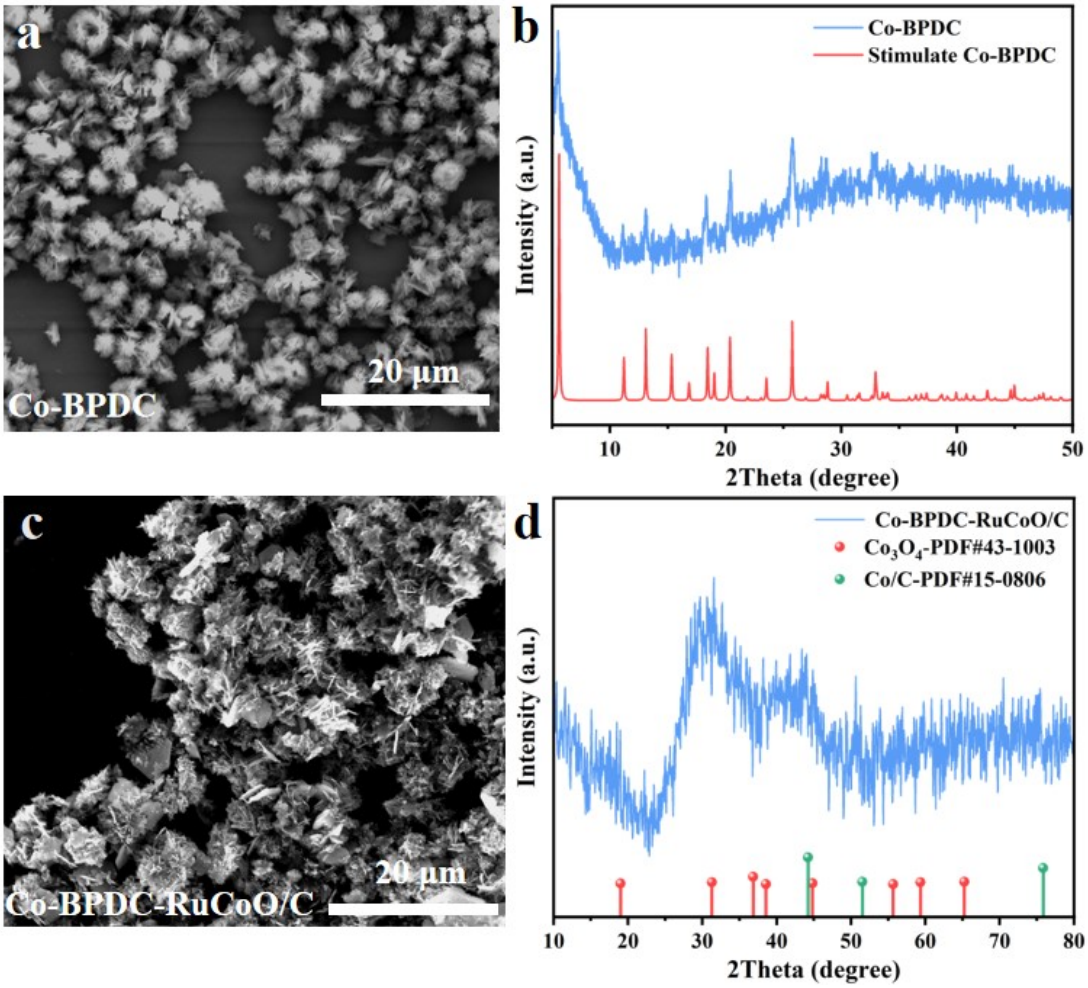

Fig. S31 (a) SEM image and (b) PXRD pattern of Co-BPDC; (c) SEM image and (d) PXRD pattern of Co-BPDC-RuCoO/C.

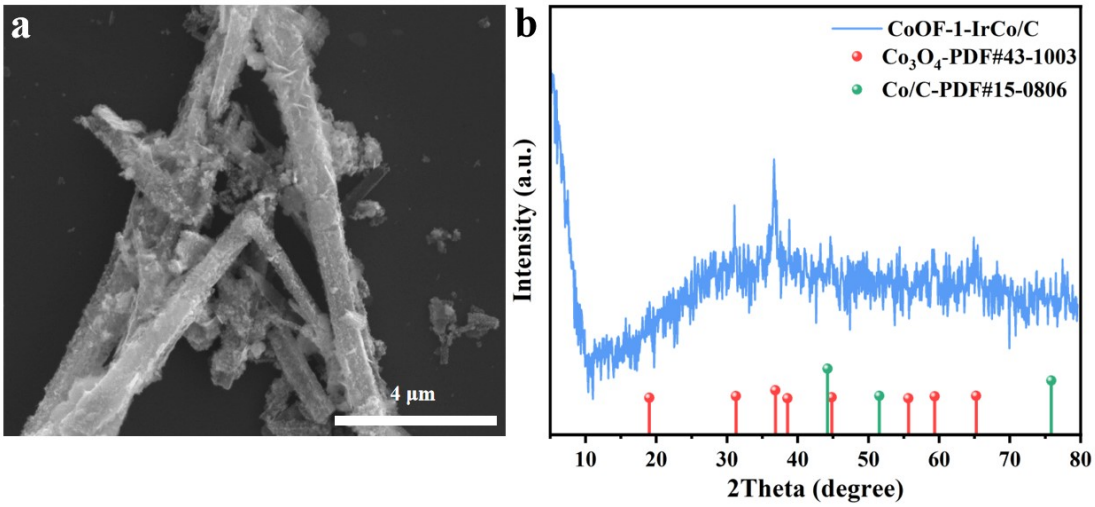

Fig. S32 (a) SEM image and (b) PXRD pattern of CoOF-1-IrCoO/C.

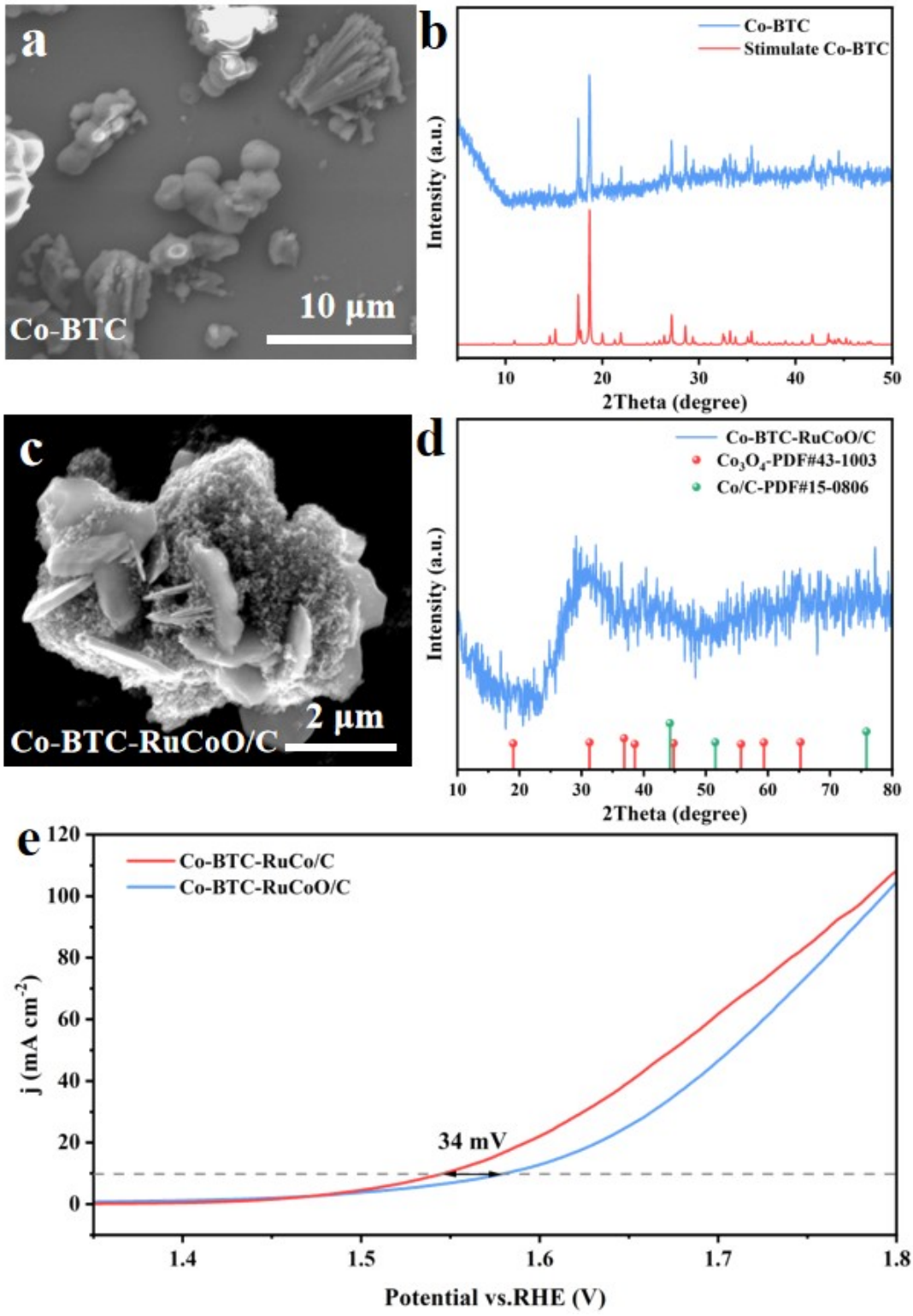

Fig. S33 (a) SEM image and (b) PXRD patterns of Co-BTC; (c) SEM image and (d) PXRD patterns of Co-BTC-RuCoO/C; (d) LSV curves of the Co-BTC-RuCo/C and Co-BTC-RuCoO/C.

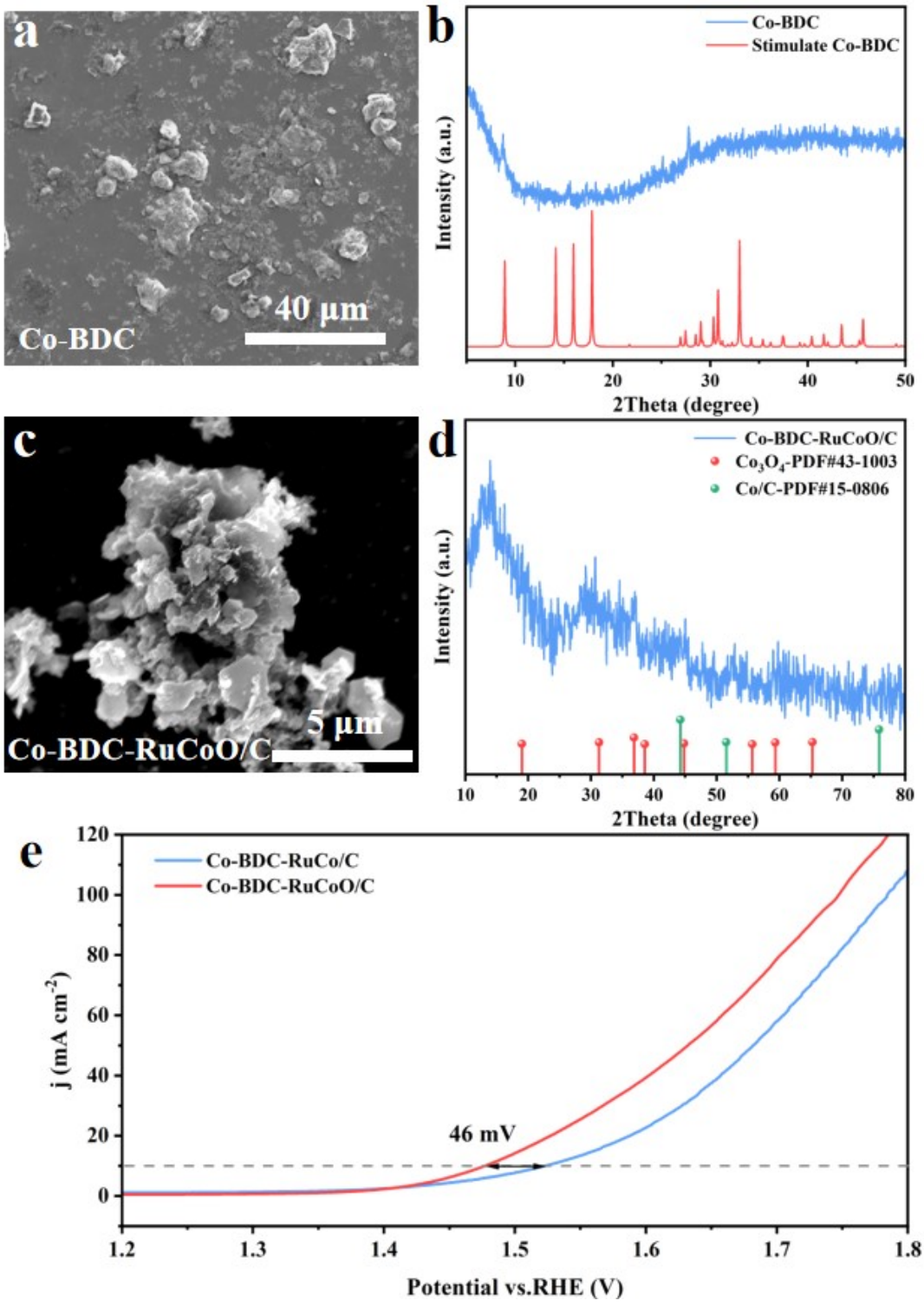

Fig. S34 (a) SEM image and (b) PXRD pattern of Co-BDC; (c) SEM image and (d) PXRD pattern of Co-BDC-RuCoO/C; (d) LSV curves of the Co-BDC-RuCo/C and Co-BDC-RuCoO/C.

Table S1 Summary of Crystal Data for CoOF-1.

Items	CoOF-1[Ref 1]
CCDC	1912147
Formula	$(C_{18}\ H_8\ Co_2\ O_{12})n$
Mass	547.15
crystal system	Tetragonal
Space group	*I4₁22*
a(Å)	15.327 (3)
b(Å)	15.327 (3)
c(Å)	12.270 (3)
α(°)	90.00
β(°)	90.00
γ(°)	90.00
V(Å^3)	2882.6 (13)
T(K)	296
Z	8
F(000)	1128.0
R_{int}	1.158
$R_1(I>2\sigma(I))$	0.0310 (1749)
wR_2(all reflections)	0.0866 (1811)

Ref 1: Li Zhong, Junyang Ding, Xian Wang, Lulu Chai, Ting-Ting Li, Kongzhao Su, Yue Hu, Jinjie Qian, Shaoming Huang CCDC 1912147: Experimental Crystal Structure Determination, 2020, DOI: 10.5517/ccdc.csd.cc225r56.

Table S2 The Content of Ru in CoOF-1-RuCoO/C by ICP-OES Measurement.

Catalysts	Relative content of Ru (wt.%)
CoOF-1-RuCoO/C-0.5	0.58
CoOF-1-RuCoO/C-3	2.92
CoOF-1-RuCoO/C-10	7.85

Table S3 Micropore Volume, Total Pore Volume and Specific Surface Area over All Prepared Catalysts.

Samples	Micropore volume (cm^3 g^{-1})	Total pore volume (cm^3 g^{-1})	Specific surface area (m^2 g^{-1})
CoOF-1	0.0116	0.112	46.4
CoOF-1-Co/C	0.0693	0.342	158.5
CoOF-1-RuCo/C	0.0675	0.370	153.0
CoOF-1-RuCoO/C	0.0548	0.373	128.0
CoOF-1-CoO	0.0145	0.138	33.7

Table S4 The Deconvolution Data of Co, O, and Ru Atoms in CoOF-1-Co/C, CoOF-1-RuCo/C, and CoOF-1-RuCoO/C.

Species	CoOF-1-Co/C	CoOF-1-RuCo/C	CoOF-1-RuCoO/C
Co^{3+} $2p_{3/2}$	779.9	780.6	780.3
Co^{2+} $2p_{3/2}$	782.6	783.5	783.2
Co^{3+} $2p_{1/2}$	795.8	796.0	795.5
Co^{2+} $2p_{1/2}$	797.9	798.4	797.8
O_L	/	529.9	529.9
O_V	/	531.6	531.1
O_A	/	533.6	532.8
C-C/C=C	284.9	284.8	284.9
C-O	286.9	286.9	286.9
C=O	289.6	289.4	289.2

Table S5 The Electrochemical Data of CoOF-1-RuCoO/C Series.

Samples	η_{10}	η_{50}	η_{100}	Tafel slope (mV dec^{-1})	C_{dl} value (mF cm^{-2})	Charge transfer resistance (Ω)
CoOF-1-Co/C	365	520	/	208	17.4	/
CoOF-1-RuCo/C	340	500	620	211	7.05	21.1
CoOF-1-RuCoO/C	247	310	349	68	3.33	25.5
CoOF-1-CoO	360	458	555	90	0.58	26.8
RuO_2	296	420	544	88	2.78	17.2

Table S6 OER Performance Comparison between CoOF-1-RuCoO/C and Other Electrode Materials.

Samples	Electrolyte	η_{10} (mV)	Tafel slope (mV dec^{-1})	Reference
CoOF-1-RuCoO/C	1.0 M KOH	247	68	**This Work**
Ir0.33@Co_3O_4	1.0 M KOH	296	68	ACS Catal., 2022, 12, 13482.
Co_3O_4 NC	1.0 M KOH	380	101	Angew. Chem., Int. Ed., 2020, 59, 7245.
Ir/Co	1.0 M KOH	273	99	J. Mater. Chem. A 2019, 7, 8376.
IrCo-NC	0.1 M KOH	330	79	ACS Catal. 2021, 11, 8837.
M-NiO@Co_3O_4	1.0 M KOH	290	68	Ind. Eng. Chem. Res., 2019, 58, 16581−16587
Ag/Co(OH)x	1.0 M KOH	250	76	Angew. Chem., Int. Ed., 2020, 59, 7245−7250
Ru-CoO	1.0 M KOH	340	84	J. Alloys Compd. 2023, 960, 170847
RuCoOx@Co/N-CNT	1.0 M KOH	350	77	J. Mater. Chem. A 2020, 8, 1229-1237

Ru/Co_3O_4–x	1.0 M KOH	280	87	ACS Catal. 2023, 13, 2462-2471
IW-Co_3O_4-RuO_2-HS	1.0 M KOH	265	55	Adv. Funct. Mater. 2022, 32, 2203206.
RuCoOx@NC	1.0 M KOH	255	69	Chem. Eng. J. 2023, 475, 146441

Table S7 Bader Charge Distribution Diagrams of Co_3O_4 and $RuCo_3O_4$/C.

Co_3O_4	Energy (e)	$RuCo_3O_4$/C	Energy (e)
Co1	-1.377449	Co1	-1.319759
Co2	-0.935283	Co2	-0.827613
Co3	-1.158593	Co3	-1.136604
Co4	-1.353029	Co4	-1.320132
Co5	-1.401538	Co5	-1.168776
Co6	**-1.308412**	Co6	-1.182825
Co7	-1.076924	Co7	-0.306701
Co8	-1.258395	Co8	-0.752725
Co9	-0.958133	Co9	-1.067499
Co10	-1.169685	Co10	-1.139388
Co11	-1.332876	**Co11**	**-1.1878**
Co12	**-1.290474**	**Ru1**	**-0.885061**
O1	0.868381	O1	0.774907
O2	0.859244	O2	0.627941
O3	0.837765	O3	0.722804
O4	0.801627	O4	0.715113
O5	0.879025	O5	0.833117
O6	0.956388	O6	0.897144
O7	0.894293	O7	0.661103
O8	0.851824	O8	0.633296

O9	0.830642	O9	0.737062
O10	0.991512	O10	0.886793
O11	0.860429	O11	0.548148
O12	0.939597	O12	0.871593
O13	0.942742	O13	0.579494
O14	0.830726	O14	0.788807
O15	0.877456	O15	0.700038
O16	0.977245	O16	0.916769
O17	**0.599811**	**O17**	**0.613913**
H1	-0.177913	H1	-0.213159

Table S8 The Electrochemical Data of Co-MOF-Ru/IrCoO/C Series.

Samples	η_{10}	η_{50}	η_{100}
ZIF-67-RuCo/C	408	563	/
ZIF-67-RuCoO/C	299	424	527
MOF-274-RuCo/C	451	/	/
MOF-274-RuCoO/C	348	460	570
Co-BPDC-RuCo/C	423	529	/
Co-BPDC-RuCoO/C	221	345	458
Co-BTC-RuCo/C	350	477	562
Co-BTC-RuCoO/C	316	446	556
Co-BDC-RuCo/C	293	452	554
Co-BDC-RuCoO/C	247	401	517
CoOF-1-IrCo/C	369	464	547
CoOF-1-IrCoO/C	259	348	433